

This article has been accepted for publication in 2023 IEEE-RAS 22nd International Conference on Humanoid Robots (Humanoids). This is the author's version which has not been fully edited and content may change prior to final publication.

Step and Timing Adaptation during Online DCM Trajectory Generation for Robust Humanoid Walking with Double Support Phases

Tobias Egle, Johannes Engelsberger, and Christian Ott

DOI: 10.1109/Humanoids57100.2023.10375152

Copyright Notice

© 2023 IEEE. Personal use of this material is permitted. Permission from IEEE must be obtained for all other uses, in any current or future media, including reprinting/republishing this material for advertising or promotional purposes, creating new collective works, for resale or redistribution to servers or lists, or reuse of any copyrighted component of this work in other works.

Step and Timing Adaptation during Online DCM Trajectory Generation for Robust Humanoid Walking with Double Support Phases

Tobias Egle, Johannes Engelsberger, and Christian Ott

Abstract—In this paper, we present a robust DCM-based online trajectory generator with step timing adaptation using MPC in addition to manipulating the ground reaction forces by the DCM tracking controller. The proposed control framework utilizes three strategies to react to disturbances: timing adaptation, footstep position adjustment, and CoP modulation. Most state-of-the-art walking controllers only address some of these aspects, and especially the timing adaptation is often neglected in the presence of double support phases as the resulting optimization problem generally becomes nonlinear. We show that we can keep the fast disturbance rejection from the DCM tracking controller while adjusting the timing and location of the footsteps via MPC if the CoP-based ankle strategy is insufficient to maintain balance. This framework is particularly relevant for robots with active control of the CoP inside the support polygon by utilizing a combination of ankle and step strategy to take full advantage of the robot’s capabilities in response to external disturbances. The method is validated in simulation on the robot kangaroo. It has lightweight, fully actuated legs and a sufficiently large contact area, making it highly suitable for a combined step time adaptation and contact force modulation approach.

I. INTRODUCTION

Bipedal locomotion holds excellent potential for navigating complex environments and allows robots to move in terrain created for humans. However, locomotion in human environments not only requires adapting to varying terrain conditions but also rapidly changing the desired trajectory, responding to external disturbances, and safely maintaining balance. Humans have developed three strategies to maintain balance: ankle, hip, and step [1]. These strategies have been applied to different extents in robotic locomotion.

To date, some of the most effective methods for walking pattern generation focus on simplified models, with particular emphasis on the linear inverted pendulum (LIPM) model [2], or reduced models like the Divergent Component of Motion (DCM) approach [3], [4]. DCM-based trajectory generation [5], in combination with a DCM tracking controller [4], has been shown to produce a stable walking motion on compliant and uneven terrain [6]. This walking controller utilizes the ankle strategy by manipulating the ground reaction forces for fast disturbance rejection. However, it is limited by the

Tobias Egle and Christian Ott are with the Automation and Control Institute, Faculty of Electrical Engineering and Information Technology, TU Wien, 1040 Vienna, Austria tobias.egle@tuwien.ac.at, christian.ott@tuwien.ac.at

Johannes Engelsberger is with the Institute of Robotics and Mechatronics, German Aerospace Center (DLR), 82234 Wessling, Germany johannes.engelsberger@dlr.de

This project has received funding from the European Research Council (ERC) under the European Union’s Horizon 2020 research and innovation programme (grant agreement No. 819358).

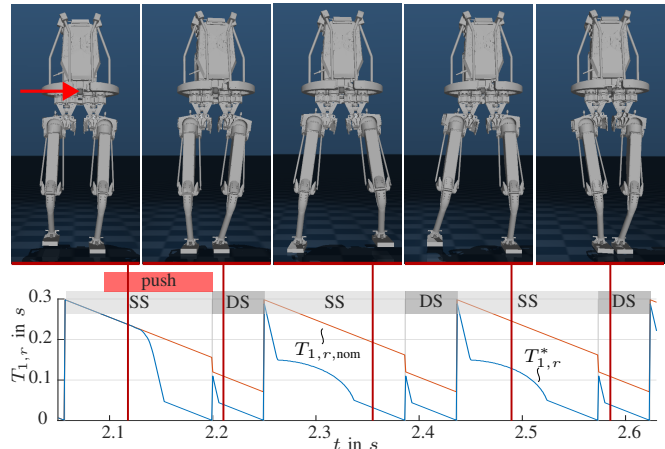


Fig. 1. Simulation snapshots of the robot kangaroo during a lateral push of $F = 300$ N for $\Delta t = 0.1$ s in the direction of the stance leg while walking forward at $v_{\text{ref}} = 0.2$ ms^{-1} . The remaining time in the first transition phase $T_{1,r}$ and the footstep positions are adjusted to retain balance.

assumption of unconstrained CoP modulation. To make the walking control more robust against disturbances, several approaches to step adaptation were presented, e.g., using the current DCM error to find an analytical solution for the next footstep adjustment [5], [7] or optimizing for the footstep position in a linear MPC approach [8]–[10]. Urata et al. [11] presented a push recovery method by utilizing non-divergence conditions of ZMP-CoM pairs through preview control. Feng et al. [12] introduced an optimal control algorithm based on the LIP model, and [13] used an analytical solution of the DCM to optimize ZMP and footstep placement simultaneously. These methods use constant step/phase timings since considering the step duration as an optimization variable for a multi-step preview would result in a nonlinear optimization problem [14]. Similarly, Aftab et al. [15] investigated ankle, hip, and stepping strategies for humanoid balance recovery with step duration adjustment using nonlinear MPC. To improve real-time capability, Khadiv et al. [16] presented a robust walking controller using convex optimization of the next step location and timing to ensure gait viability by specifying a desired distance between the DCM and the swing foot landing point. Griffin et al. [17] developed a walking stabilization approach using an analytical DCM-based recursive algorithm that involved step timing and location adjustment for the humanoid robot Atlas. Shafiee et al. [18] present an MPC-based step and timing adaptation using an exponential interpolation of the ZMP trajectory, which is only active in the single support phase. The next step and, more importantly, the phase duration is not adjusted in the double support phase. Similar works based

on the LIPM that consider the ankle and step strategy with time adjustment compute the step and time adjustment in a sequential analytical solution [19] or with a quadratically constrained quadratic program [20]. Mesesan et al. [21] recently introduced an online DCM trajectory adaptation for push recovery using DCM tracking control and an analytical solution for the next footstep position, which is active in the double support phase but uses constant phase timings.

For several recent robots, such as Digit [22] or Kangaroo [23], which have lightweight, fully actuated legs, and a sufficiently large contact area, a combination of ankle and step strategy is desirable to take full advantage of the robot's capabilities and avoid the need for constant stepping. This paper proposes a combination of MPC and DCM tracking control to implement both ankle and stepping strategies. The MPC provides optimal step position and timing to correct the error the DCM controller cannot compensate for because of the limited CoP manipulation in the support polygon. With this framework, the suggested control law considers three aspects to maintain balance: timing of steps, step location, and manipulation of ground reaction forces. Most state-of-the-art walking controllers consider only some of these aspects.

The main contribution of this paper is the presentation of a new method of combining ankle and step strategy with time adaptation. In addition, we explicitly consider double support phases, which, combined with the ankle strategy, allow the robot to quickly eliminate minor disturbances without taking a step. This enables precise tracking of a pre-planned footstep plan.

The paper is organized as follows: Section II recalls previous works on DCM trajectory generation and Sec. III gives an overview of the proposed control framework. Section IV describes the footstep planner and Sec. V introduces the step and timing optimization framework. We evaluate the proposed methods in simulation with the robot kangaroo in Sec. VI. Possible extensions and future work are discussed in Sec. VII and Sec. VIII concludes the paper.

II. PRELIMINARIES

The walking trajectory generation is based on the concepts of three-dimensional Divergent Component of Motion (DCM) and Virtual Repellent Point (VRP) introduced in [4]. The DCM ξ is defined as a linear combination of the CoM position x and velocity \dot{x} as

$$\xi = x + b\dot{x}, \quad (1)$$

where the time constant $b = \sqrt{\Delta z/g}$ is given by the average CoM height over the ground Δz and the gravity constant g . The VRP v encodes the total force f on the CoM as

$$f = \frac{m}{b^2} (x - v), \quad (2)$$

where m is the total mass. We find the DCM dynamics by differentiating (1) and inserting the CoM dynamics $\ddot{x} = f/m$ with (2) as

$$\dot{\xi} = \frac{1}{b} (\xi - v). \quad (3)$$

Being defined as a general three-dimensional point, the VRP is not constrained to the ground or the support polygon. However, it is related to the CoP and for the following trajectory generation, we choose the vertical projection of the VRP onto the ground to be within the support polygon.

A. DCM Trajectory Generation

An efficient computation of the DCM trajectory is given in [24]. The walking motion is divided into n_φ transition (single and double support) phases. For each phase φ with duration T_φ , we specify the VRP trajectory $v_\varphi(t)$ as a spatially linear interpolation between a VRP start point $v_{\varphi,0}$ and a VRP end point $v_{\varphi,T}$ to allow for double support phases and pre-planned CoP movement during single support phases. Given $v_\varphi(t)$, we solve (3) as a terminal value problem to obtain

$$\xi_\varphi(t) = \alpha_\varphi(t)v_{\varphi,0} + \beta_\varphi(t)v_{\varphi,T} + \gamma_\varphi(t)\xi_{\varphi,T}, \quad (4)$$

where $t \in [0, T_\varphi]$ and $\alpha_\varphi(t)$, $\beta_\varphi(t)$, and $\gamma_\varphi(t)$ are nonlinear coefficients in time that depend on the temporal interpolation of $v_\varphi(t)$ (see Appendix). To ensure continuity of the trajectory, the transition phase start and end points of adjacent phases are linked, i.e., $v_{\varphi,0} = v_{\varphi-1,T}$ and $\xi_{\varphi,0} = \xi_{\varphi-1,T}$. We specify a terminal condition $\xi_{n_\varphi,T} = \xi_f$ at the end of the last transition phase and recursively compute the DCM waypoints in matrix form:

$$\Xi = \Xi C_V V + \Xi c_\xi \xi_f^T, \quad (5)$$

where and the $n = n_\varphi + 1$ VRP and DCM waypoints are collected in the matrices $V = [v_1 \dots v_n]^T$ and $\Xi = [\xi_1 \dots \xi_n]^T$, respectively. A detailed analytical computation of the matrix ΞC_V and vector Ξc_ξ can be found in [24].

B. DCM tracking control

Due to the naturally stable CoM dynamics, only the unstable first-order DCM dynamics must be controlled. Engelsberger et al. [4] suggested tracking the reference DCM trajectory by aiming at a closed-loop dynamics of the form

$$\dot{\xi} - \dot{\xi}_{\text{ref}} = -K_\xi (\xi - \xi_{\text{ref}}), \quad (6)$$

which is stable for a positive diagonal matrix K_ξ . Inserting the DCM dynamics (3) and the DCM reference velocity into the desired dynamics (6) and solving for the input v yields the tracking control law of the form

$$v = v_{\text{ref}} + (I + bK_\xi) (\xi - \xi_{\text{ref}}), \quad (7)$$

where v_{ref} is the reference VRP position and $e_\xi = \xi - \xi_{\text{ref}}$ is the DCM tracking error.

C. Separation into Ankle and Step Strategy

Mesesan et al. [21] proposed to split the current DCM error $\tilde{\xi}(t) = \xi(t) - \xi_{\text{ref}}(t)$ into two parts as

$$\tilde{\xi}(t) = \tilde{\xi}_{\text{ankle}}(t) + \tilde{\xi}_{\text{step}}(t), \quad (8)$$

where $\tilde{\xi}_{\text{ankle}}$ is the part that the ankle strategy can correct and $\tilde{\xi}_{\text{step}}$ is the part that needs to be corrected by the step strategy. According to the mentioned CoP relation, we want to keep the horizontal coordinates (xy) of the VRP

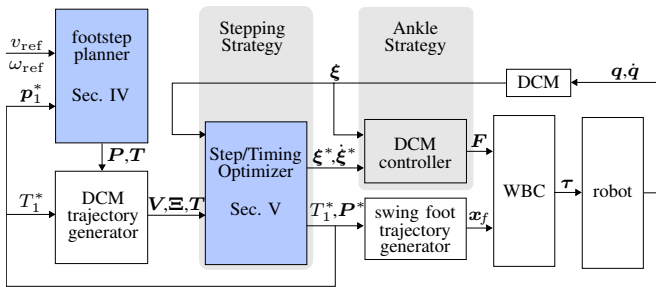


Fig. 2. Outline of the proposed walking trajectory generation and control framework. The main contributions of this paper are highlighted in blue.

in the support polygon. Placing the VRP over the center of a rectangular foot of length $2l$ and width $2w$, the set $\tilde{V} = \{\tilde{v} = (x \ y \ 0)^T \mid -l \leq x \leq l, -w \leq y \leq w\}$ is defined as the set of VRP adjustments that remain in the support polygon, and \tilde{V}_{ankle} is the set of VRP adjustments usable by the ankle strategy defined as

$$\tilde{V}_{\text{ankle}} = \mathbf{R}_{z,j} \otimes \tilde{V} := \{\mathbf{R}_{z,j} \tilde{v} \mid \tilde{v} \in \tilde{V}\}, \quad (9)$$

where the rotation matrix $\mathbf{R}_{z,j} \in SO(3)$ specifies the orientation of the j -th footstep. The corresponding set of DCM errors $\tilde{\xi}_{\text{ankle}}$ correctable by \tilde{V}_{ankle} until the end of the current step is obtained by evaluating the recursive DCM computation for the current and next transition phases. Due to the linear relation between VRP and DCM, we write the DCM recursion for the first two phases according to (4) in terms of displacements $\tilde{\xi}_{\varphi} = \xi_{\varphi} - \xi_{\varphi,\text{ref}}$ as

$$\begin{aligned} \tilde{\xi}_1(t) &= \alpha_1(t)\tilde{v}_1 + \beta_1(t)\tilde{v}_2 + \gamma_1(t)\tilde{\xi}_2 \\ \tilde{\xi}_2 &= \alpha_{2,0}\tilde{v}_2 + \beta_{2,0}\tilde{v}_3 + \gamma_{2,0}\tilde{\xi}_3. \end{aligned} \quad (10)$$

Here, we evaluated the second transition phase at $t = 0$ and expressed the transition phase start and end point displacements $\tilde{v}_{\varphi,0}$, $\tilde{v}_{\varphi,T}$ and $\tilde{\xi}_{\varphi,T}$ in terms of VRP and DCM waypoint displacements \tilde{v}_i and $\tilde{\xi}_i$, respectively. Assuming that the DCM waypoint error $\tilde{\xi}_3$ and thus the required VRP displacement \tilde{v}_3 at the end of the next transition phase shall become zero, we obtain $\tilde{\xi}_{\text{ankle}}$ by evaluating (10) for all $\tilde{v}_i \in \tilde{V}_i$ where $i \in \{1, 2\}$ as

$$\tilde{\xi}_{\text{ankle}}(t) = \alpha_1(t)\tilde{V}_1 + (\beta_1(t) + \gamma_1(t)\alpha_{2,0})\tilde{V}_2. \quad (11)$$

Projecting the current DCM error $\tilde{\xi}$ onto $\tilde{\xi}_{\text{ankle}}$ minimizes $\|\tilde{\xi}_{\text{step}}\|$ as illustrated in Fig. 4. This ensures that the step strategy activates only if $\tilde{\xi}$ is not contained in $\tilde{\xi}_{\text{ankle}}$.

III. OVERVIEW OF THE CONTROL FRAMEWORK

An overview of the walking control framework is given in Fig. 2. The inputs of the footstep planner are the linear and angular velocity $(v_{\text{ref}}, \omega_{\text{ref}})$ of the torso, from which a sequence of footsteps $\mathbf{P} = [\mathbf{p}_1 \dots \mathbf{p}_{n_{\text{fs}}}]^T$ with corresponding timings $\mathbf{T} = [T_1 \dots T_{n_{\text{fs}}}]^T$ is planned. At the touchdown of the swing foot, the footstep plan is updated with the optimized position \mathbf{p}_1^* , and in each time step, the current transition phase time is updated with T_1^* . Consecutively, the reference VRP and DCM trajectories are computed according to Sec. II-A. The Step/Timing Optimizer computes, based

on the DCM error $\tilde{\xi}_1$, the optimized first transition phase time, DCM waypoints, and foot positions. The commanded DCM position and velocity are passed to the DCM controller, which computes the desired force on the CoM as input for the whole-body controller according to (7). With the optimized phase timing and foot positions, the swing foot trajectories are computed using a fifth-order and a sixth-order polynomial interpolation in the horizontal and vertical direction, respectively. We utilize a QP-based inverse dynamics whole-body controller [25] to compute the joint torques that are supplied to the robot. The current DCM of the robot is used as an input to the Step/Timing Optimizer and DCM tracking controller.

IV. FOOTSTEP PLANNER

We assume a level ground and no environmental constraints such as obstacles or stepping stones for the footstep planner. Possible extensions are discussed in Sec. VII.

A. Nominal Footstep Plan

Based on the desired walking speed v_{ref} , we select the walking cycle time T_c and stance percentage $s_p \in [0, 1]$ according to empirical observations for humans [26]. The walking cycle time T_c is scaled by a factor $c_r \in [0.5, 0.7]$ to fit the robot's kinematic and dynamic capabilities, i.e., the robot rather makes smaller and more frequent steps compared to a human. Thus, we obtain the stance and swing times as

$$\begin{aligned} T_{\text{st}} &= s_p c_r T_c, \\ T_{\text{sw}} &= (1 - s_p) c_r T_c, \end{aligned} \quad (12)$$

and subsequently, the single and double support times result in $T_{\text{SS}} = T_{\text{sw}}$ and $T_{\text{DS}} = (T_{\text{st}} - T_{\text{sw}})/2$, respectively. The walking step length is given by

$$l = T_c v_{\text{ref}}/2. \quad (13)$$

Similarly, we define a desired angular (yaw) velocity ω_{ref} of the torso and obtain the relative angle between two consecutive footsteps as

$$\theta = T_c \omega_{\text{ref}}/2. \quad (14)$$

With these parameters and a nominal step width w , we generate a footstep plan with n_{fs} footstep frames $\mathbf{H}_{f,j} \in SE(3)$ representing footstep positions \mathbf{p}_j and rotations $\mathbf{R}_{z,j}(\theta_j) \in SO(3)$. An illustration of the footstep plan is shown in Fig. 3. The walking direction is to the right, and the rotation of the footsteps is omitted for conciseness.

B. Nominal Footstep Plan with Disturbance

We update the first foot position to coincide with the current foot position of the robot. In case of strong disturbances, the current foot position may no longer be compatible with the planned footsteps due to the kinematic limitations of the robot. To obtain feasible foot positions $\mathbf{p}_{j,\text{feas}}$, we project the next planned footstep positions \mathbf{p}_j consecutively onto a feasible set of footstep positions $P_{j,\text{feas}}$ defined by a polygonal approximation of a semicircular region with radius r relative to the previous foot position. In Fig. 3, the first planned footstep position (\mathbf{p}_1 , left foot) is updated with the

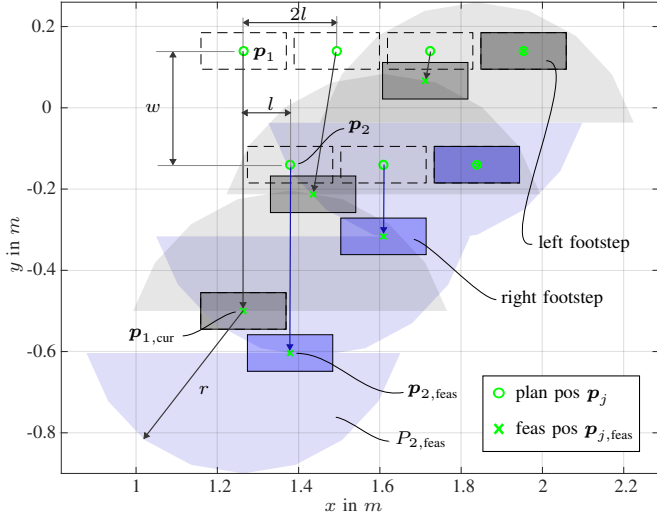


Fig. 3. Projection of footstep plan onto feasible foot positions. The left footsteps are displayed in gray, and the right ones are highlighted in blue. Similarly, the feasible set of foot positions for the next left or right footstep is shown in light gray or blue, respectively. The reference footstep plan is illustrated in dashed lines.

current foot position $p_{1,cur}$. Thereby, the robot cannot step to the next planned footstep (p_2 , right foot) due to kinematic constraints. The footstep is projected onto $P_{2,feas}$ to yield the new footstep position $p_{2,feas}$. Accordingly, the remaining footsteps are projected to feasible positions ensuring that the footstep plan remains valid even in the case of significant disturbances.

V. STEP/TIMING OPTIMIZER

In the following section, we introduce the DCM trajectory generation as an optimization problem in Sec. V-A, extend it with time adjustment in the first transition phase in Sec. V-B, combine it with the ankle strategy in Sec. V-C and formulate it as a Quadratic Program in Sec. V-D. The DCM trajectory generation presented in Sec. II-A provides an efficient way to compute the DCM trajectory for a given set of VRP waypoints and a DCM terminal point. However, it is of limited use as an online trajectory generator since the DCM waypoints are computed in a backward recursion and yield a unique DCM start point, which will not coincide with the current DCM of the robot. If the DCM error $\tilde{\xi}$ becomes larger than the error that the DCM tracking controller can compensate for (see Sec. II-C), the trajectory becomes infeasible.

A. DCM Trajectory Generation as an Optimization Problem

A possible solution would be to formulate the trajectory generation as an optimization problem and compute adjusted VRP and DCM waypoints compliant with the current DCM of the robot as an initial condition. Due to the unstable DCM dynamics, this formulation also requires a DCM terminal condition to be set at the end of the predefined sequence of steps. In the following, we omit the subscript φ for the transition phase for better readability. First, we specify a

linear interpolation of the VRP trajectory as

$$v(t) = \left(1 - \frac{t}{T}\right) v_0 + \frac{t}{T} v_T \quad \forall \varphi \in \{1, \dots, n_\varphi\}, \quad (15)$$

and solve the DCM Dynamics as an initial value problem, which gives

$$\begin{aligned} \xi(t) = & \underbrace{\left(1 - \frac{t+b}{T} - e^{\frac{t}{b}} \left(1 - \frac{b}{T}\right)\right)}_{\alpha(t)} v_0 \\ & + \underbrace{\left(\frac{t+b}{T} - e^{\frac{t}{b}} \frac{b}{T}\right)}_{\beta(t)} v_T + \underbrace{e^{\frac{t}{b}}}_{\gamma(t)} \xi_0, \end{aligned} \quad (16)$$

and the DCM at the end of transition phase time T as

$$\xi_T = \alpha_T v_0 + \beta_T v_T + \gamma_T \xi_0, \quad (17)$$

where $\xi_T = \xi(T)$, $\alpha_T = \alpha(T)$, $\beta_T = \beta(T)$ and $\gamma_T = \gamma(T)$. The DCM and VRP waypoints are defined as optimization variables, and we specify (17) and a DCM initial and terminal condition as constraints. We introduce additional constraints on the VRP waypoints to ensure that the kinematic limits of the robot, i.e., step length and width, are not exceeded and obtain a feasible DCM trajectory for a given current DCM of the robot. However, this approach does not allow for timing adjustment in a convex optimization as the solution to the DCM dynamics (17) is nonlinear in T and would involve the multiplication of optimization variables.

B. Allowing for Time Adjustment in First Transition Phase

The adjustment of the VRP waypoints of the current phase corresponds to a manipulation of the ground reaction forces. Leaving this task to the DCM tracking controller, we can keep v_1 and v_2 constant thus allowing for time adjustment in the first transition phase by solving the problem of multiplication of optimization variables. However, the coefficients α_T , β_T and γ_T are still nonlinear in the transition phase time T . Since (17) is a linear combination between VRP and DCM, we formulate the equation for all phases n_φ in terms of waypoint displacements as

$$\tilde{\xi}_i = \alpha_{T,i-1} \tilde{v}_{i-1} + \beta_{T,i-1} \tilde{v}_i + \gamma_{T,i-1} \tilde{\xi}_{i-1}, \quad (18)$$

with $i \in \{2, \dots, n_{wp}\}$. Here, $\tilde{\xi}_i$ and \tilde{v}_i are the deviations between the optimized and the nominal DCM and VRP waypoints, respectively. For this computation, the transition phase times are assumed to be constant. Due to the nonlinearity introduced by the multiplication of optimization variables, we can only adjust the timing or the VRP displacements in each transition phase with convex optimization. Thus, consistent with (18), we keep the timing constant for all except for the first transition phase. In the first equation of (18), we adjust the timing and introduce this approximation in order to obtain a linear equation in the optimization variables in the following and proceed with a QP. The exact solution leads to a more general nonlinear optimization problem. With the constraint that the difference in phase time between two iterations is limited, i.e., $|T_1^* - T_{1,prev}^*| \leq 0.01$ s,

this assumption is reasonable, as demonstrated in simulation in Sec. VI. Since we keep the VRP waypoints of the current phase constant, i.e., the displacements \tilde{v}_1 and \tilde{v}_2 are zero, the first equation in (18) simplifies to

$$\tilde{\xi}_2 = e^{\frac{T}{b}} \tilde{\xi}_1. \quad (19)$$

In this way, we eliminate the nonlinear coefficients $\alpha_{T,1}$ and $\beta_{T,1}$ from equation (18) and obtain with the variable substitution $\tau = e^{\frac{T}{b}}$ a linear relation in the optimization variables. We adjust the first transition phase time T_1 and the previewed footsteps to cancel the part of the DCM error that the DCM tracking controller can not correct for in the current footstep. This enables the robot to efficiently manipulate the ground reaction forces for fast disturbance rejection and minimize the required step adjustment for the DCM error $\tilde{\xi}$.

C. Mixed Ankle and Step Strategy (DCM Error Separation)

This section aims to apply both the ankle and step strategies by separating the DCM error into two parts. The step strategy compensates one part, while the other is left to the DCM tracking controller. Thus, we define the part that is corrected by the step strategy as

$$\tilde{\xi}_1(t_1) = \tilde{\xi}_{\text{step}}^{\text{rt}}(t_1) + \tilde{\xi}_{\text{step}}^{\text{ed}}(t_1), \quad (20)$$

where t_1 is the local time in the first transition phase, $\tilde{\xi}_{\text{step}}^{\text{rt}}$ is the DCM error due to an offset in the reference trajectory, and $\tilde{\xi}_{\text{step}}^{\text{ed}}$ is the DCM error due to an external disturbance. As described earlier, the computation of the DCM waypoints in a backward recursion according to (5) leads to discontinuities in the time evolution of the first DCM waypoint $\xi_1(t)$ in case of discrete changes of the footstep positions. However, changes of the pre-planned footstep positions are necessary to change the reference velocity or to keep a constant number of previewed footsteps. To avoid these discontinuities affecting the commanded DCM $\xi_1^*(t)$, the DCM offset

$$\tilde{\xi}_{\text{step}}^{\text{rt}}(t_1) = \xi_1^*(t_1) - \xi_1(t_1) \quad (21)$$

is fully compensated by the stepping strategy. The reference DCM $\xi_1(t_1)$ is computed according to (4) with the last optimized time $T = T_{1,\text{prev}}^*$ as

$$\xi_1(t_1) = \alpha(t_1)\mathbf{v}_1 + \beta(t_1)\mathbf{v}_2 + \gamma(t_1)\xi_2. \quad (22)$$

Similarly, the current VRP $\mathbf{v}_1(t_1)$ is obtained by evaluating (15) for the first transition phase as

$$\mathbf{v}_1(t_1) = \left(1 - \frac{t_1}{T_1^*}\right) \mathbf{v}_1 + \frac{t_1}{T_1^*} \mathbf{v}_2. \quad (23)$$

To utilize the ankle strategy, the current DCM error

$$\tilde{\xi}(t_1) = \xi(t_1) - \xi_1^*(t_1) \quad (24)$$

is projected onto $\tilde{\mathbf{E}}_{\text{ankle}}$ and thus separated into two parts, as shown in Fig. 4. Only the DCM error $\tilde{\xi}_{\text{step}}^{\text{ed}}$ due to an external disturbance, which is computed according to Sec. II-C, is compensated by the stepping strategy (see (20)). Thus, if there is no DCM offset, i.e., $\xi_1^* = \xi_1$, and the current DCM error $\tilde{\xi}$ is inside the red region in Fig. 4, i.e., inside $\tilde{\mathbf{E}}_{\text{ankle}}$, only the ankle strategy is active.

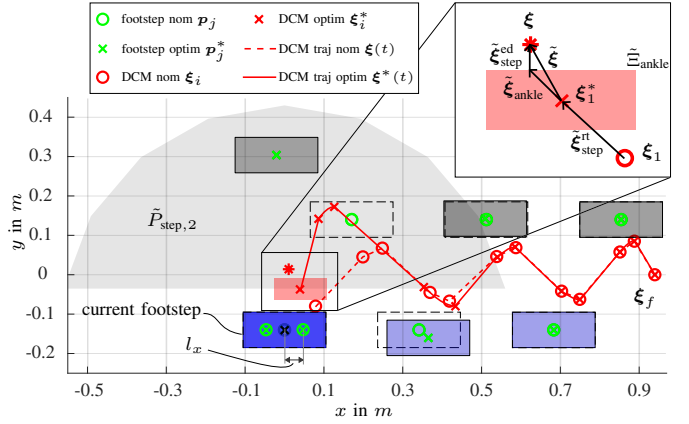


Fig. 4. Reference and optimized DCM trajectory and footstep plan during a single support phase. The current footstep is highlighted in dark blue, and the previewed right and left footsteps are displayed in light blue and gray, respectively. The reference footstep plan is illustrated with dashed lines. The DCM error $\tilde{\xi}$ is split into two parts, as illustrated in the magnification.

D. Foot Location and Timing Adaptation

To reduce the size of the optimization problem, the VRP waypoints are expressed in terms of foot positions. The definition of the VRP waypoints \mathbf{v}_i depends on whether the current phase is a single support phase (cSS) or a double support phase (cDS):

$$\mathbf{v}_i = \mathbf{p}_j + \mathbf{R}_{z,j} [(-1)^i \Delta x \ 0 \ \Delta z]^T \quad \forall i \in \{2, \dots, n_{\text{wp}}\}$$

with $j = \begin{cases} \lceil i/2 \rceil & \text{for cSS} \\ \lfloor i/2 + 1 \rfloor & \text{for cDS} \end{cases}$ and $\Delta x = \begin{cases} l_x & \text{for cSS} \\ -l_x & \text{for cDS.} \end{cases}$ (25)

Here, j is the index used to select the corresponding reference foot position, l_x represents a constant VRP offset from the footstep center in the x -direction corresponds to predefined CoP movement from heel to toe in the single support phase. The rotation matrix $\mathbf{R}_{z,j}$ specifies the orientation of the footstep. For simplicity, we specify $\Delta x = 0$ for the preview footsteps as shown in Fig. 4. Writing (25) in terms of displacements and inserting into (18) yields

$$\tilde{\xi}_i = \begin{cases} (\alpha_{T,i-1} + \beta_{T,i-1}) \tilde{\mathbf{p}}_j + \gamma_{T,i-1} \tilde{\xi}_{i-1} & \text{for SS} \\ \alpha_{T,i-1} \tilde{\mathbf{p}}_j + \beta_{T,i-1} \tilde{\mathbf{p}}_{j+1} + \gamma_{T,i-1} \tilde{\xi}_{i-1} & \text{for DS,} \end{cases} \quad (26)$$

with i and j defined as in (25). The optimization problem is formulated as a quadratic program as

$$\begin{aligned} \min_{\tau, \tilde{\mathbf{p}}_j, \tilde{\xi}_i} \quad & w_\tau |\tau - \tau_{\text{nom}}|^2 + \sum_{j=k}^{k+n_{\text{pfs}}} \|\tilde{\mathbf{p}}_j\|_{\mathbf{w}_p}^2 + \sum_{i=2}^{n_{\text{wp}}} \|\tilde{\xi}_i\|_{\mathbf{w}_\xi}^2 \\ \text{s.t.} \quad & (19), (26), \\ & e^{\frac{T_{\text{min}}}{b}} \leq \tau \leq e^{\frac{T_{\text{max}}}{b}}, \\ & \tilde{\mathbf{p}}_j \in \tilde{\mathbf{P}}_{\text{step},j}, \\ & \text{with } k = \begin{cases} 2 & \text{for cSS} \\ 3 & \text{for cDS,} \end{cases} \end{aligned} \quad (27)$$

where $\tau = e^{\frac{T}{b}}$, n_{pfs} is the number of previewed footsteps, and n_{wp} is the number of waypoints.

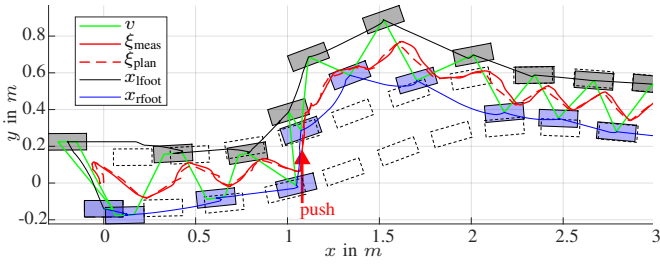


Fig. 5. Top view of a footstep plan and trajectories from a push recovery simulation. The left footsteps are shown in grey, and the right footsteps are highlighted in blue. The reference step plan is illustrated in dashed lines.

For the timing of the footsteps both the distance between the current position of the swing foot and the intended target position and the maximum acceleration of the swing foot need to be considered. Here, for simplicity, the minimum transition phase time is determined by an empirically determined maximal velocity of the foot $v_{f,\max}$ and the remaining distance to the target position $\mathbf{X}_{ft,t}$ as

$$T_{\min} = \max \left(|\mathbf{X}_{ft,t} - \mathbf{X}_{ft}| / v_{f,\max} \right). \quad (28)$$

The adjusted foot positions are obtained as

$$\mathbf{p}_j^* = \mathbf{p}_j + \tilde{\mathbf{p}}_j^* \quad \forall j = \{k, \dots, k + n_{\text{pfs}}\}, \quad (29)$$

with k defined as in (27). Similarly, the adjusted DCM waypoints are given by

$$\xi_i^* = \xi_i + \tilde{\xi}_i^* \quad \forall i = \{2, \dots, n_{\text{wp}}\}, \quad (30)$$

and the current adjusted DCM results in

$$\xi_1^*(t_1) = \xi_1(t_1) + \tilde{\xi}_1(t_1). \quad (31)$$

With the optimized remaining phase time

$$T_{1,r}^* = b \ln(\tau), \quad (32)$$

the first transition phase time evaluates to

$$T_1^* = t_1 + T_{1,r}^*. \quad (33)$$

To compute the next commanded DCM, we evaluate (16) with the current VRP $\mathbf{v}_1(t_1)$ and adjusted DCM $\xi_1^*(t_1)$ from (23) and (31), respectively, and the remaining time $T_{1,r}^*$ as

$$\xi_1^*(t_1 + t_s) = \alpha(t_s)\mathbf{v}_1(t_1) + \beta(t_s)\mathbf{v}_2 + \gamma(t_s)\xi_1^*(t_1), \quad (34)$$

where t_s is the sample time and t_1 is the local time in the first transition phase. The next commanded DCM position and velocity (via (3)) are passed to the DCM controller.

VI. SIMULATION RESULTS

In this section, we present the simulation results with the robot kangaroo using the MuJoCo simulation environment [27]. The height of kangaroo is 145 cm with a mass of 40 kg, each leg has a mass of 12.5 kg, and its feet are 21 cm long and 9 cm wide. The quadratic program for the step timing adjustment (27) and the whole-body controller are solved with qpSWIFT [28] within less than 1 ms on a 3.8 GHz AMD Ryzen 7 processor.

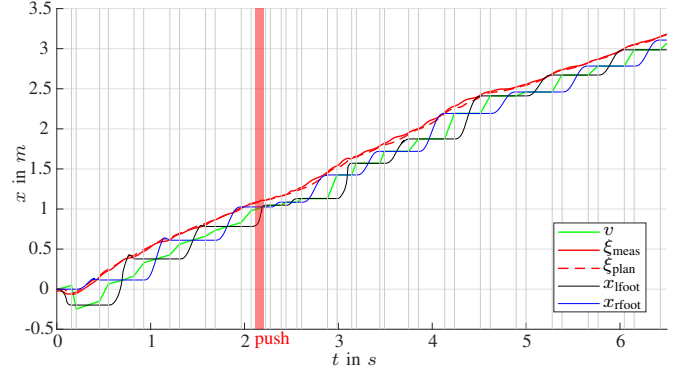


Fig. 6. Sagittal (in the walking direction) trajectories during the push recovery simulation. The vertical grid lines show the change between two transition phases.

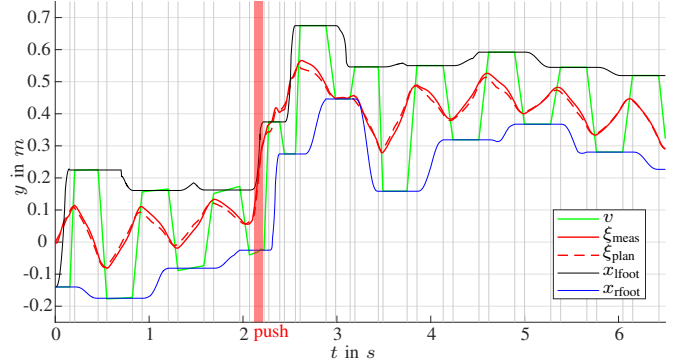


Fig. 7. Lateral trajectories during the push recovery simulation. The vertical grid lines show the change between two transition phases.

A. Push Recovery

Figure 5 shows the top view of a simulation, where the robot is walking forward with the reference velocity $v_{\text{ref}} = 0.4 \text{ ms}^{-1}$ and the SS and DS timings and step length according to Sec. IV. The reference angular velocity alternates between $\omega_{\text{ref}} = \pm 0.2 \text{ s}^{-1}$. After a first step adjustment to compensate for the initial DCM error, the robot follows the footstep plan. In the first steps, desired CoP movement corresponding to VRP movement in the support area during the single support phase is demonstrated. This predefined CoP movement is well suited for the nominal gait if, e.g., heel- or toe-off walking is desired. In the case of disturbance rejection due to external pushes, however, the choice of the VPR in the center of the foot has proven to be the most robust since, here, the DCM controller has the largest margin of possible VRP adjustments in all directions.

The robot is pushed at $t = 2.1 \text{ s}$ with $F = 200 \text{ N}$ for $\Delta t = 0.1 \text{ s}$ in the lateral direction, causing it to leave the desired step plan. The controller adjusts the step position to react to the disturbance and return to the desired step plan. The sagittal (walking) direction is hardly disturbed, as seen in Fig. 6. Here, it can be observed particularly well that the frequency of the footsteps is increased during the disturbance rejection. The vertical grid lines show the change between two transition phases. Figure 7 shows how the controller adjusts the footsteps in the lateral direction to recover from the disturbance. The time adjustment in the first transition phase is shown in more detail in Fig. 8. Without disturbance,

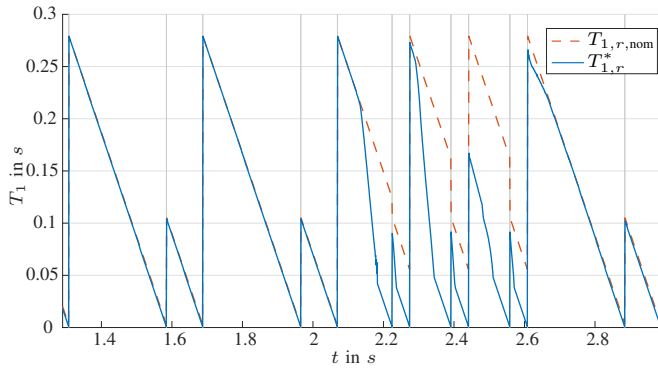


Fig. 8. Adjustment of the first transition time T_1 in the time period around the push. The vertical grid lines show the change between two transition phases.

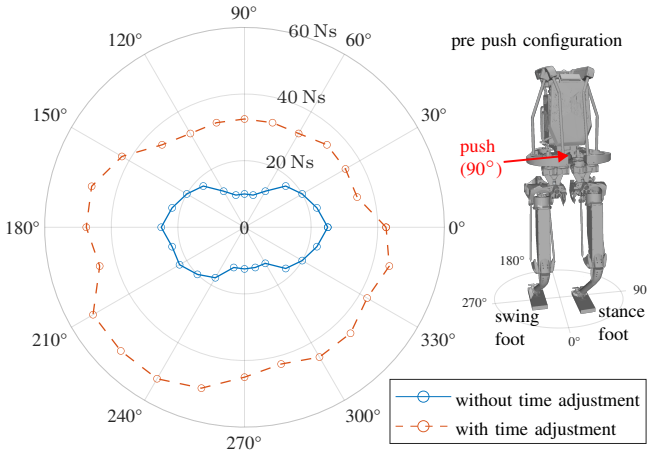


Fig. 9. Comparison of the maximal recoverable disturbance impulse for a push as in Fig. 1 while walking forward at $v_{\text{ref}} = 0.2 \text{ ms}^{-1}$. The push occurs in the last two-thirds of the left foot stance phase for $\Delta t = 0.1 \text{ s}$.

the remaining phase time $T_{1,r}^*$ follows the nominal remaining time $T_{1,r,\text{nom}}$ and reduces linearly until the end of the phase. Due to the disturbance, the controller adjusts the phase duration according to the constraints given in (27) until the remaining time is smaller than $T_{1,r}^* < 0.05 \text{ s}$ where it is reduced linearly again to ensure that the feet have sufficient time to reach the target position.

The increased robustness due to time adjustment, which allows to recover from more significant disturbances, is shown in Fig. 9. Since the robot is standing on its left foot at the instance of the push, as can be seen in Fig 1, the maximal disturbances that can be compensated are smaller to the left (in the direction of the stance leg) than to the right. The maximum recoverable push in this configuration equals 525 N to the rear right.

B. Change in Reference Velocity

Figure 10 shows the tracking of a desired reference walking velocity v_{ref} . During steady-state walking, the measured velocity of the robot follows the reference velocity, with oscillations based on DCM dynamics. In case of abrupt velocity changes, a transient response takes place. The reference velocity determines the timing of the walking phases and the step length. As a result, the step plan and the timing of the steps are instantly modified. Since the robot cannot

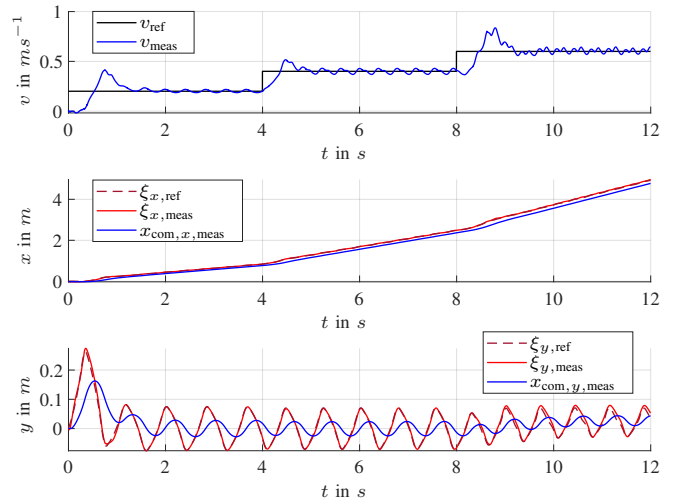


Fig. 10. Discrete changes in the reference velocity result in smooth DCM trajectories. The CoM naturally follows the DCM according to (1).

always instantly react to an updated step plan, e.g., in the double support phase, the step position and timing must be adjusted to accelerate and compensate for the missed velocity change such that the integral for reference and measured velocity is equal. After the transient phase, the robot follows the reference speed again. Since the step timing adaptation compensates for the speed change, the reference DCM trajectory remains continuous, as shown in the lower two plots in Fig. 10.

VII. EXTENSIONS/FUTURE WORK

The semicircular feasible step region shown in Figs. 3 and 4 is only a subset of the actual possible target positions of the feet since the QP limits us to convex boundary conditions. A C-shaped region around the current footstep and, thus, a possible crossing of the feet, which would contribute significantly to the stability of the movement, cannot be implemented with a QP. However, the proposed method can be readily extended by more refined approaches that find convex regions allowing for a crossing of the legs. The parameterization of these convex regions by heuristic, model-based, or model-free approaches is part of future work.

Another possible extension would be to intersect the feasible step region by kinematic constraints with the feasible step region by environmental constraints, such as stepping stones or obstacles. With the proposed multi-step preview controller, the DCM and footstep adjustments can anticipate for future obstacles or constraints and thus enable robust walking in cluttered environments or on stepping stones.

VIII. CONCLUSION

In this paper, we have presented a DCM-based online trajectory generation framework for walking that adjusts to perturbations in three different ways: time adaptation, footstep position adjustment, and modulation of ground reaction forces. The advantages of the proposed method are the utilization of the ankle strategy in combination with the adjustment of the current phase duration, the adaptation of

multiple previewed footsteps, constraints on footstep placement, and the presence of double support phases. The simulations showed robust recovery from external disturbances while tracking a desired footstep plan and the ability to respond to discrete changes in reference velocity. The supplementary video contains multiple simulations demonstrating the proposed walking control with the robot kangaroo.

APPENDIX

VRP AND DCM TRAJECTORY IN THE TRANSITION PHASE

We define the VRP trajectory as a spatially linear interpolation between a VRP start point $\mathbf{v}_{\varphi,0}$ and end point $\mathbf{v}_{\varphi,T}$ as

$$\mathbf{v}_{\varphi}(t) = (1 - f_{\varphi}(t)) \mathbf{v}_{\varphi,0} + f_{\varphi}(t) \mathbf{v}_{\varphi,T}, \quad (35)$$

where $\mathbf{v}_{\varphi,0} = \mathbf{v}_{\varphi}(0)$, $\mathbf{v}_{\varphi,T} = \mathbf{v}_{\varphi}(T_{\varphi})$ and $t \in [0, T_{\varphi}]$ is the local time of the transition phase φ . Generally, low-order polynomial splines are used as temporal interpolation functions $f_{\varphi}(t)$ for each transition phase. The smoothness of the DCM and CoM trajectories depends on the order n_p of the splines, e.g., a linear interpolation is given by:

$$f_{\varphi}(t) = t/T_{\varphi}. \quad (36)$$

Higher-order interpolation schemes are presented in [5]. Inserting the VRP trajectory (35) into (3) gives the DCM dynamics for the transition phase φ :

$$\dot{\xi}_{\varphi}(t) = \frac{1}{b} \left(\xi_{\varphi}(t) - \mathbf{v}_{\varphi}(t) \right). \quad (37)$$

Multiplying (37) by the integrating factor $e^{-t/b}$ facilitates partial integration and results in the DCM trajectory:

$$\begin{aligned} \xi_{\varphi}(t) = & \underbrace{\left(1 - \sigma_{\varphi}(t) - e^{-\frac{t-T_{\varphi}}{b}} (1 - \sigma_{\varphi,T}) \right)}_{\alpha_{\varphi}(t)} \mathbf{v}_{\varphi,0} + \\ & + \underbrace{\left(\sigma_{\varphi}(t) - e^{-\frac{t-T_{\varphi}}{b}} \sigma_{\varphi,T} \right)}_{\beta_{\varphi}(t)} \mathbf{v}_{\varphi,T} + \underbrace{e^{-\frac{t-T_{\varphi}}{b}}}_{\gamma_{\varphi}(t)} \xi_{\varphi,T}, \end{aligned}$$

$$\text{where } \sigma_{\varphi}(t) = \sum_{j=0}^{n_p} \left(b^j f_{\varphi}^{(j)}(t) \right), \quad (38)$$

with $\sigma_{\varphi,T} = \sigma_{\varphi}(T_{\varphi})$. Here, $f_{\varphi}^{(j)}(t)$ denotes the j -th derivative of function $f_{\varphi}(t)$ and $\xi_{\varphi,T} = \xi_{\varphi}(T_{\varphi})$ is the DCM end point.

REFERENCES

- [1] F. B. Horak and L. M. Nashner, "Central programming of postural movements: Adaptation to altered support-surface configurations," *Journal of Neurophysiology*, vol. 55, no. 6, pp. 1369–1381, 1986.
- [2] S. Kajita, F. Kanehiro *et al.*, "The 3D linear inverted pendulum mode: A simple modeling for a biped walking pattern generation," in *Proc. IEEE Int. Conf. Robot. Automat.*, vol. 1, 2001, pp. 239–246.
- [3] T. Takenaka, T. Matsumoto *et al.*, "Real time motion generation and control for biped robot -1st report: Walking gait pattern generation-," in *Proc. IEEE/RSJ Int. Conf. Intell. Robots Syst.*, 2009, pp. 1084–1091.
- [4] J. Engelsberger, C. Ott *et al.*, "Three-Dimensional Bipedal Walking Control Based on Divergent Component of Motion," *IEEE Transactions on Robotics*, vol. 31, no. 2, pp. 355–368, 2015.
- [5] J. Engelsberger, G. Mesesan *et al.*, "Smooth trajectory generation and push-recovery based on Divergent Component of Motion," in *Proc. IEEE/RSJ Int. Conf. Intell. Robots Syst.*, 2017, pp. 4560–4567.
- [6] G. Mesesan, J. Engelsberger *et al.*, "Dynamic Walking on Compliant and Uneven Terrain using DCM and Passivity-based Whole-body Control," in *Proc. IEEE-RAS 19th Int. Conf. Humanoid Robots*, 2019, pp. 25–32.
- [7] M. Khadiv, S. Kleff *et al.*, "Stepping stabilization using a combination of DCM tracking and step adjustment," in *Proc. 4th International Conference on Robotics and Mechatronics (ICROM)*, 2016, pp. 130–135.
- [8] H. Diedam, D. Dimitrov *et al.*, "Online walking gait generation with adaptive foot positioning through Linear Model Predictive control," in *Proc. IEEE/RSJ Int. Conf. Intell. Robots Syst.*, 2008, pp. 1121–1126.
- [9] A. Herdt, N. Perrin *et al.*, "Walking without thinking about it," in *Proc. IEEE/RSJ Int. Conf. Intell. Robots Syst.*, 2010, pp. 190–195.
- [10] M. Shafiee-Ashtiani, A. Yousefi-Koma *et al.*, "Robust bipedal locomotion control based on model predictive control and divergent component of motion," in *Proc. IEEE Int. Conf. Robot. Automat.*, 2017, pp. 3505–3510.
- [11] J. Urata, K. Nshiwaki *et al.*, "Online walking pattern generation for push recovery and minimum delay to commanded change of direction and speed," in *Proc. IEEE/RSJ Int. Conf. Intell. Robots Syst.*, 2012, pp. 3411–3416.
- [12] S. Feng, X. Xinjilefu *et al.*, "Robust dynamic walking using online foot step optimization," in *Proc. IEEE/RSJ Int. Conf. Intell. Robots Syst.*, 2016, pp. 5373–5378.
- [13] T. Kamioka, H. Kaneko *et al.*, "Simultaneous Optimization of ZMP and Footsteps Based on the Analytical Solution of Divergent Component of Motion," in *Proc. IEEE Int. Conf. Robot. Automat.*, 2018, pp. 1763–1770.
- [14] P. Kryczka, P. Kormushev *et al.*, "Online regeneration of bipedal walking gait pattern optimizing footstep placement and timing," in *Proc. IEEE/RSJ Int. Conf. Intell. Robots Syst.*, 2015, pp. 3352–3357.
- [15] Z. Aftab, T. Robert *et al.*, "Ankle, hip and stepping strategies for humanoid balance recovery with a single Model Predictive Control scheme," in *Proc. 12th Int. Conf. Humanoid Robots*, 2012, pp. 159–164.
- [16] M. Khadiv, A. Herzog *et al.*, "Walking Control Based on Step Timing Adaptation," *IEEE Transactions on Robotics*, vol. 36, no. 3, pp. 629–643, 2020.
- [17] R. J. Griffin, G. Wiedebach *et al.*, "Walking stabilization using step timing and location adjustment on the humanoid robot, Atlas," in *Proc. IEEE/RSJ Int. Conf. Intell. Robots Syst.*, 2017, pp. 667–673.
- [18] M. Shafiee, G. Romualdi *et al.*, "Online DCM Trajectory Generation for Push Recovery of Torque-Controlled Humanoid Robots," in *Proc. IEEE-RAS 19th Int. Conf. Humanoid Robots*, 2019, pp. 671–678.
- [19] Y. Kojio, Y. Omori *et al.*, "Footstep Modification Including Step Time and Angular Momentum Under Disturbances on Sparse Footholds," *IEEE Robotics and Automation Letters*, vol. 5, no. 3, pp. 4907–4914, Jul. 2020.
- [20] J. Ding, X. Xiao *et al.*, "Robust Gait Synthesis Combining Constrained Optimization and Imitation Learning," in *2020 IEEE/RSJ International Conference on Intelligent Robots and Systems (IROS)*, Oct. 2020, pp. 3473–3480.
- [21] G. Mesesan, J. Engelsberger *et al.*, "Online DCM Trajectory Adaptation for Push and Stumble Recovery during Humanoid Locomotion," in *Proc. IEEE Int. Conf. Robot. Automat.*, 2021, pp. 12780–12786.
- [22] "Digit Humanoid Robot," <https://agilityrobotics.com/robots>.
- [23] A. Roig, S. K. Kothakota *et al.*, "On the Hardware Design and Control Architecture of the Humanoid Robot Kangaroo," in *6th Workshop on Legged Robots during the Int. Conf. Robot. Automat.*, 2022.
- [24] G. Mesesan, J. Engelsberger *et al.*, "Convex Properties of Center-of-Mass Trajectories for Locomotion Based on Divergent Component of Motion," *IEEE Robotics and Automation Letters*, vol. 3, no. 4, pp. 3449–3456, 2018.
- [25] J. Engelsberger, G. Mesesan *et al.*, "Torque-Based Dynamic Walking - A Long Way from Simulation to Experiment," in *Proc. IEEE Int. Conf. Robot. Automat.*, 2018, pp. 440–447.
- [26] G. Cappellini, Y. P. Ivanenko *et al.*, "Motor patterns in human walking and running," *Journal of Neurophysiology*, vol. 95, no. 6, pp. 3426–3437, 2006.
- [27] E. Todorov, T. Erez *et al.*, "MuJoCo: A physics engine for model-based control," in *Proc. IEEE/RSJ Int. Conf. Intell. Robots Syst.*, 2012, pp. 5026–5033.
- [28] A. G. Pandala, Y. Ding *et al.*, "qpSWIFT: A Real-Time Sparse Quadratic Program Solver for Robotic Applications," *IEEE Robotics and Automation Letters*, vol. 4, no. 4, pp. 3355–3362, 2019.